Integrated Nano, 2026, Vol. X, Iss. X, 60-75

DOI: 10.62184/in.jin010420261

Research Article

SCIENCE PARK PUBLISHER

Integrated Nano

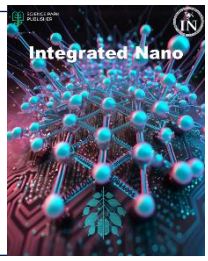

Novel approaches to enhance electrical conductivity of nanoscale PEDOT: PSS layers

Amrita Chakraborty, Aaron DiFilippo, Anshu Madwesh, Calvin Hong, Sheena Deivasigamani, Marius Orlowski*

ECE Department, Virginia Polytechnical Institute and State University, Blacksburg, Virginia 24061, USA

Received: 05, 02, 2025; Accepted: 02, 12, 2025; Published: 15, 01, 2026

Abstract

This investigation expands on our earlier work to increase PEDOT:PSS (P-S) electrical conductivity. We explore a variety of methods, such as the use of mono- and multi-atomic layer graphene, the deposition of multiple P-S layers, doping with metal nanoparticles (Ag and Cu), and acid treatment. According to our research, P-S multilayers can be optimally deposited and treated with nitric acid to get better outcomes than those obtained using graphene and metal nanoparticles. When compared to the employment of graphene layers and metal nanoparticles, this optimized method not only improves the electrical conductivity of P-S but also has benefits in terms of cost-effectiveness, greater stability, and decreased mistakes. To achieve these results, optimization parameters including etching time, etchant concentration, and spin speed are essential. In comparison to single-layer P-S of the same thickness, the optimized multilaminar P-S treated with nitric acid results in a significant drop in sheet resistance from over 1 MΩ/sq to 6.85 Ω/sq, which translates to electrical conductivity of 0.17 S/cm to 15,701 S/cm, respectively. In order to reduce dependability problems brought on by environmental factors, we also manage lamina aging.

Keywords: Conductive polymers; PEDOT:PSS; Metal nanoparticles; Topical and bulk doping; Graphene; Acid treatment

1. Introduction

The main objective of this paper is to create organic electrodes for nonvolatile ReRAM memory arrays [1] that are embedded with copper or silver particles on flexible substrates rather than traditional silicon wafers. In our previous work [2], we attempted to enhance the conductivity of P3HT polymer laminas but were unable to achieve conductivities higher than several S/cm. As a result, we turned to PEDOT:PSS layers (P-S), which have been reported to reach electrical conductivities as high as 4380 S/cm with acid treatment.

A key benefit of PEDOT:PSS (P-S) lies in its ability to have its electrical conductivity finely adjusted from 10^{-3} S/cm for as-cast films to over 4000 S/cm for films treated with secondary dopants or solvents such as dimethyl sulfoxide, ionic liquids, or ethylene glycol (EG). These treatments enhance the conductivity by reorganizing the PEDOT chains into more conductive domains and reducing the insulating effect of PSS content at the surface. Additionally, P-S films exhibit high optical transparency in the visible spectrum, making them suitable for use in transparent conductive electrodes.

P-S has been widely explored as a replacement for traditional inorganic transparent conductive oxides (TCOs) such as indium tin oxide (ITO) in flexible and stretchable electronic devices [3]. Unlike ITO, which is brittle and expensive, P-S is highly flexible, lightweight, and compatible with a variety of substrates, including plastics, textiles, and paper. This makes it particularly well-suited for applications in flexible displays,

wearable electronics, and organic photovoltaics (OPVs) [3, 4]. In organic solar cells, P-S is commonly used as a hole transport layer (HTL) or as a transparent anode. Its work function can be adjusted to align with the energy levels of the active layer, enhancing charge extraction and boosting device efficiency. Similarly, in organic light-emitting diodes (OLEDs), P-S serves as an effective hole injection layer (HIL), thereby enhancing device performance and stability [5].

Despite its many advantages, P-S faces several challenges that limit its widespread adoption. These include its relatively low conductivity compared to metals, susceptibility to moisture and environmental degradation, and the acidic nature of the PSS, which can corrode metal electrodes over time. Recent research has focused on addressing these issues through the development of new formulations, additives, and post-treatment methods. For example, the incorporation of graphene, carbon nanotubes, or metal nanoparticles has been shown to enhance the conductivity and stability of P-S films [3]. Increased electrical conductivity of P-S has been obtained by treating the lamina with acid [6].

A P-S lamina treated with concentrated H_2SO_4 acid at 120 °C yielded a conductivity of 4380 S/cm [7], almost comparable to that of ITO and Ga- or Al-doped ZnO. However, the narrow interval of temperature required for manufacturing electrodes with such high conductivity poses challenges for ensuring a reproducible process. High-temperature and acid-based treatments can lead to issues such as inconsistent results and safety concerns when working at temperatures up to 120 °C. In contrast, S.J. Yun and co-workers [8] reported a P-S lamina treated with 14 M HNO_3 at 300 K, producing an electrical conductivity of 4100 S/cm under much more stable and reproducible conditions.

To eliminate excess PSS and enhance the crystallinity of PEDOT chains, mild organic acids such as formic acid, acetic acid, and methanesulfonic acid have been employed. Ouyang [6] showed that treatment with formic acid increased the conductivity of P-S to over 3000 S/cm. To enhance P-S conductivity, dopants in the form of ionic liquids have been employed. These liquids act as plasticizers, improving the ordering of PEDOT chains and reducing Coulombic interactions between PEDOT and PSS. Xia and Ouyang [9] reported a conductivity of over 1400 S/cm using ionic liquid treatment. Surfactants like Zonyl and salts such as lithium triflate (LiTf) have been used to modify the morphology of P-S films, leading to improved conductivity. Zhou et al. [9] demonstrated that Zonyl treatment increased conductivity to 2000 S/cm. Heating P-S films at elevated temperatures (typically 100–200 °C) can improve conductivity by removing residual water and inducing structural reorganization of PEDOT chains. Crispin et al. [10] (2006) showed that thermal annealing at 120 °C increased conductivity by a factor of 10. Exposure to solvent vapors (e.g., DMSO, EG, or methanol) can induce phase separation and improve conductivity. This method is particularly useful for avoiding damage to underlying layers in multilayer devices. Kim et al. [11] reported a conductivity of 1400 S/cm after EG vapor treatment. Mechanical stretching aligns PEDOT chains in the direction of strain, enhancing conductivity along the stretching axis. Okuzaki et al. [12] achieved a conductivity of 880 S/cm by stretching P-S films. The addition of conductive nanomaterials like carbon nanotubes (CNTs), graphene, or metal nanoparticles (such as silver nanowires) to P-S can lead to a substantial improvement in conductivity. Zhang et al. [13] demonstrated that adding graphene to P-S increased conductivity to 2500 S/cm. Layer-by-layer (LbL) deposition of P-S with other conductive materials (e.g., polyelectrolytes or nanoparticles) can create highly conductive multilayer structures. Li et al. [14] achieved a conductivity of 3000 S/cm using LbL assembly with silver nanoparticles. Immersing P-S films in strong acids (sulfuric acid) or strong bases (NaOH) can remove excess PSS and improve conductivity. However, this method may compromise the mechanical stability of the films. Fan et al. [15] reported a conductivity of 4380 S/cm after sulfuric acid treatment. Electrospinning P-S into nanofibers can create highly conductive networks with improved mechanical flexibility. Chen et al. [16] achieved a conductivity of 1200 S/cm using electrospun P-S fibers. Laser treatment can locally enhance conductivity by inducing structural changes in P-S films without damaging the substrate. Kim et al. [17] demonstrated laser-induced conductivity enhancement up to 2000 S/cm. It remains an open question as to which of these enhancement methods is most suitable for use as electrodes in ReRAM applications.

We presented a new technique for creating conductive organic electrodes with doped P-S polymer laminas in our earlier research [18]. Our research demonstrated these electrodes'

remarkable potential by demonstrating their patternability and strong adhesion to various substrates, including flexible materials like oxidized silicon wafers and Mylar. Simple oxygen plasma cleaning was used to ensure substrate adhesion. To prevent chemical degradation of P-S when exposed to typical solvents employed in photolithography chemistry, we structured the laminas using a dummy silver pellicle as a protective layer. One of the main conclusions from reference [2] is that numerous P-S depositions can significantly boost electrical conductivity (in excess of two orders of magnitude) without appreciably thickening the lamina. In order to better understand the functions of PEDOT (the conducting phase) and PSS (the non-conductive phase) within the deposited P-S material, we noticed a basic dependence between the number of P-S pellicles and the sheet resistance, which led to the emergence of an exponential decrease in the sheet resistance with number of P-S laminas. When no other improvement techniques are applied, using more than six P-S pellicle layers yields only diminishing returns in terms of sheet resistance reduction. The present study pioneers the systematic exploration of sequential enhancement techniques in multilayer P-S stacks, revealing that strategic combinations of layer deposition and staggered HNO_3 etching can achieve record-low sheet resistance (2 Ω/sq) and uncover non-linear, synergistic effects not observed with single treatments. While previous work examined individual methods in isolation, our approach maps an unexplored parameter space where layer order and treatment sequence govern interlayer connectivity and performance, providing a proof-of-concept and a foundation for future optimization. The synergistic effects of the various enhancement techniques are summarized in Tables 6 and 7.

Additionally, in our earlier work [2, 18, 19], we investigated surface doping soft-baked P-S laminas with Cu nanoparticles (Cu NPs), which demonstrated even another astounding hundredfold improvement in electrical conductivity. In this paper we find a significant counteractive impact, though, as the two conductivity enhancing techniques Cu NPs doping and multiple P-S pellicles did not add up as expected. In other words, combining these two methods did not result in any additional or cumulative benefits.

In this research, we aim to assess the compatibility of different methods for improving conductivity and evaluate possible synergistic effects, continuing from earlier work [2, 19]. We report that the use of silver nanoparticles, whether through topical application or bulk doping, shows encouraging results. However, it is worth noting that when paired with acid treatment, no further substantial enhancements are observed. Even more importantly we demonstrate that Ag nanoparticles offer no advantage compared to Cu NPs, but only if the latter are applied topically in an ethanol solution.

This study is structured in four sections: The second section reviews the electrode fabrication, where we start with a brief overview of the basic fabrication steps for patterning and depositing P-S layers. We also explore techniques described in our previous work [18] to improve these laminas' electrical conductivity. Following this, we provide an in-depth discussion of the treatment by acid processing, including the preparation, integration, and application of Cu and Ag nanoparticle dispersions, as well as single- and multilayer graphene stacks. The Results Section begins by examining the impacts of both topical and bulk doping of P-S with silver nanoparticles, as well as the distinct effects of nitric, sulfuric, and phosphoric acids (HNO_3, H_3PO_4, and H_2SO_4). In this initial part, we focus on the outcomes of each method individually. Later in the main Results Section, the synergistic benefits achieved by integrating these techniques with the multi-lamina P-S deposition process are explored. Finally, in the Summary Section, we present the key findings and conclusions.

2. Fabrication of the P-S electrode

The development of organic electrodes started with commercial P-S dispersion in water. Organic laminas were applied to cleaned substrates, such as flexible Mylar substrates and silicon wafers covered with a 550 nm thick oxide layer, using this dispersion. We used the spin-coating procedure for lamina deposition, with spin speeds between 400 rpm and 3500 rpm. For multilayer P-S stacks, the selection of spin speed was crucial, as it needed to be carefully calibrated for each layer, including speed ramps, to obtain the targeted lamina thickness and reduce sheet resistance effectively. The P-S laminas have been designed to provide a step in order to precisely quantify the lamina thickness. We demonstrated the use of photolithography to pattern highly conductive polymer laminas in the earlier publication [2]. This procedure used a new flow that depended on the insertion of sacrificial metal

Integrated Nano, 2026, Vol. X, Iss. X, 60-75
DOI: 10.62184/in.jin010420261

Research Article

layers. We effectively resolved adhesion problems and showed that highly conductive P-S laminas can be printed on flexible substrates such as Mylar as well as silicon wafer with precisely calibrated process recipes. This development creates opportunities for the use of flexible electronics. As indicated in Table 1, the spinning speed and the quantity of P-S pellicles determine the thickness of the P-S layer. For example, a 3×lamina P-S deposited at 1500, 2000, and 3000 rpm for the first, second, and third layer, respectively, results in a total lamina thickness of 72 nm. This is just 7 nm thicker than a single P-S layer of 65 nm deposited at 1500 rpm, deviating significantly from the expected additive sum of 150 nm (=65+56+29). The non-additive thickness in multilayer P-S laminas is primarily due to the stratified morphology of each layer. As established in our previous work [2, 19], during spin-coating, the water-insoluble PEDOT-rich phase sinks to the bottom of the film, while the water-soluble PSS-rich phase segregates to the top. When a subsequent layer is deposited, its solvent (water) partially redissolves this PSS-rich upper region of the previous layer instead of simply adding a discrete new film. This dissolution and interlayer mixing prevent the total stack thickness from being a linear sum of individual layer thicknesses. An AFM image of the measurement of the film's thickness is shown in Figure 1(a) along with an optical microscopy image of a step of a patterned P-S film (Figure 1(b)).

We used protective layers, namely PVD-deposited silver (Ag) thin laminas, to pattern the P-S. Because they shielded the lamina from exposure to UV radiation and chemical reagents, these layers were essential to the photolithography process. The photo resist AZ 5214E-IR was developed after the intended pattern was exposed as part of the photolithography process. After that, an HNO_3: H_2O solution was used to etch the exposed Ag areas. Rinsing was the next step, and then oxygen plasma treatment was used to remove the P-S layer. Essentially, the earlier study [2] covered important phases of the P-S lamina production process, from precision photolithography-based patterning to deposition and uniformity testing, with a focus on attaining higher electrical conductivity.

A comparative analysis using phosphoric, nitric, and sulfuric, with concentrations varied from 0% to 100% was performed in an effort to optimize acid treatment methods for P-S samples. The acid treatment lasted anywhere from one second to sixty seconds. The sheet resistance of P-S was significantly reduced by our approach, which used each acid at a 100% concentration level and a brief 2 s treatment. Only one layer of the P-S material received the acid treatment in this first experiment. P-S silicon wafer samples are submerged in the acid solution for the predetermined duration after the acid concentration has been precisely measured. To maintain the reliability of the results, the samples were immediately rinsed with deionized (DI) water to remove any remaining acid.

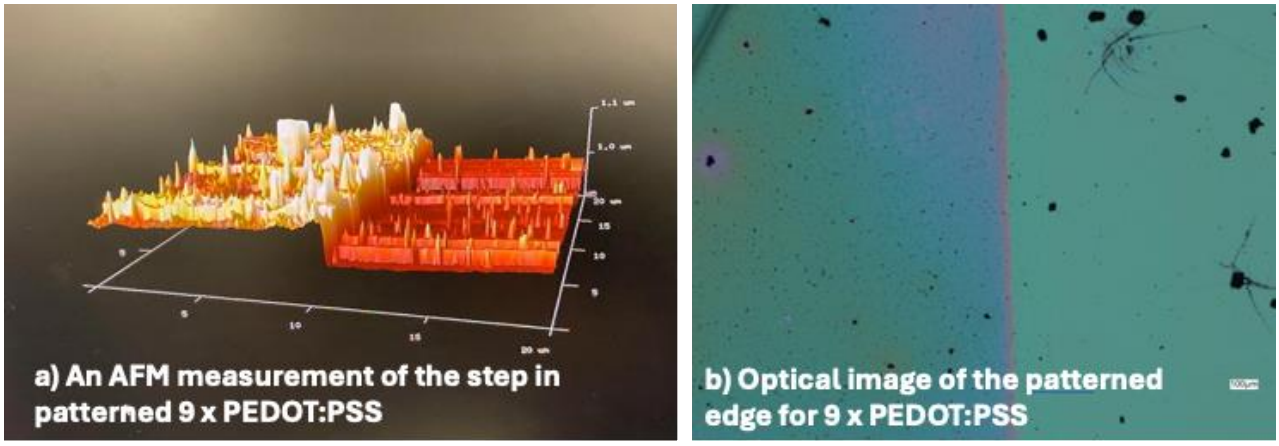

Figure 1. a) An AFM image of the 9×P-S stack step used to gauge the thickness of the film, and b) shows an optical microscope image of a 9× P-S stack's patterned edge.

Integrated Nano, 2026, Vol. X, Iss. X, 60-75
DOI: 10.62184/in.jin010420261

Research Article

The primary function of the acid treatment is to eliminate PSS from the top layer, regardless of whether it targets one or more P-S layers. As shown in Figure 2, the residue consists of a layer that is mostly made of PEDOT and occasionally contains residual PSS inclusions.

We used both topical and bulk doping techniques to incorporate silver nanoparticles (Ag NPs) into multilayer P-S in our tests. For bulk doping, 10 mL of P-S solution and 5 mg of Ag NPs were combined to create a 0.5 mg/mL solution. After stirring for 1 h, the mixture was sonicated for an additional hour. The same stirring and sonication procedure used in the bulk doping method was utilized to create a dispersion of Ag NPs and Cu NPs in ethanol at a concentration of 0.5 mg/mL for surface doping. After Ag NPs were dispersed in ethanol, the surface of the P-S layer was spin-coated at 1500 rpm. Our previous work with Cu NPs [2, 18, 19] helped us determine that the concentration of Ag NPs should be 0.5 mg/ml. In previous work [18], we investigated two distinct concentrations of Cu NPs, 0.2 mg/mL and 0.5 mg/mL, and determined that the latter yielded the most favorable outcomes. When working with Ag NPs, we chose to use the same concentration (0.5 mg/mL) to ensure uniformity.

Regarding the Ag NPs, we acquired two powder samples from Sky Springs Nanomaterials, Inc.: one containing nanoparticles sized between 20 and 30 nm and the second with sizes from 50 to 60 nm. The conductivity of P-S was found to be larger for the larger-sized nanoparticles (see the next section). The ultimate enhancing technique considered in this paper involves inserting single and triple layer [19] graphene between the P-S laminas and the oxidized silicon wafer.

The triple lamina graphene is available as an isolated sample on square 1 cm^2 square-shaped slabs of oxidized Si wafers from the firm Graphenea [20]. The structure is created by directly stacking three graphene monolayers on top of each other.

The four-probe measuring method was used to determine the conductivity (represented by σ) or sheet resistance (represented by R_{sq}) of the P-S layers [21]. Sheet resistance, conductivity, and electrical characteristics are all connected and can be represented using Equation (1):

$$\sigma = \frac{1}{R_{sq} \times t} \qquad (1)$$

Suppose, for example, that a pristine P-S lamina with a thickness (t) of 55 nm with a sheet resistance R_{sq} of 10^6 Ω/sq was spin-coated at 2000 rpm. This value of sheet resistance is equivalent to a conductivity of σ = 0.18 S/cm based on Equation (1).

Table 1. Measured thickness in nm for a 1-layer P-S, 3-layer P-S, 6-layer P-S, 9-layer, and 12-layer P-S stack at different spinning speeds.

P-S # rpm	1× 1500	1× 2000	1× 3000	3× 1500,3000,1500	3× 1500,2000,3000	6× 1500,2000,4×3000	9× 1500,2000,7×3000
Thick [nm]	65	56	29	85	72	118	151

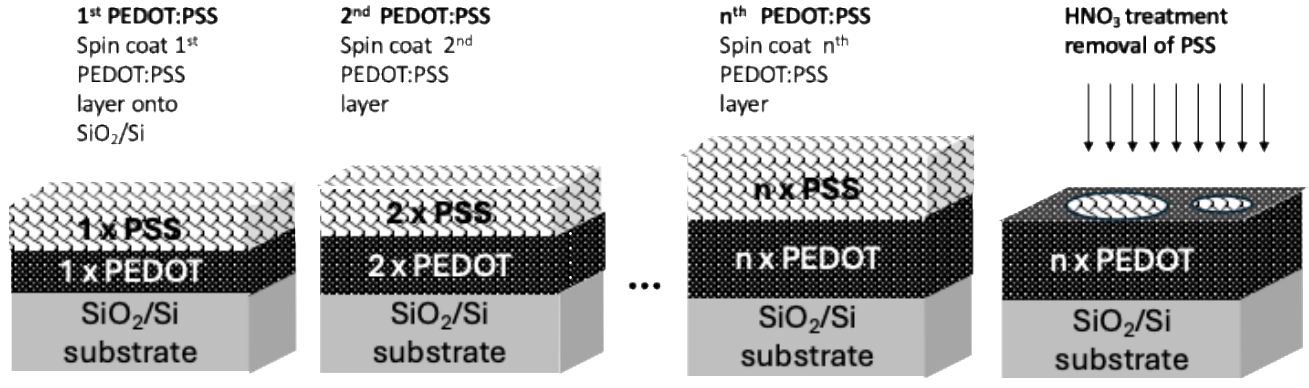

Figure 2. Shows the procedures involved in treating multilayer P-S laminas with acid. Only PSS inclusions remain in the PEDOT phase after the top part of PSS is removed by the acid treatment.

Integrated Nano, 2026, Vol. X, Iss. X, 60-75
DOI: 10.62184/in.jin010420261

Research Article

3. Experimental results and analysis

We began our study by using phosphoric, sulfuric, and nitric acids to examine how an acid treatment affects a P-S single layer. After two seconds of 100% concentration, the values of sheet resistance for the three acid treatments are shown in Table 2. As shown in Table 2, sulfuric and nitric acids demonstrate significantly better performance compared to phosphoric acid, with at least a fivefold improvement, and nitric acid holds a slight edge over sulfuric acid. Even after applying a 60% concentration of acid for one minute, the observed decreases in sheet resistance remained constant over a range of acid concentrations and treatment times. Our next focused on the nitric acid method because it consistently produced the best outcomes. We investigated various treatment times of 1, 2, 3, 30, 40, and 60 s when working with HNO_3 at 100% concentration. According to our research, sheet resistance was only little impacted by treatment time variation, with the 1-2 s treatment exhibiting a minor benefit.

Next, we investigate how the concentration of HNO_3 affects its capacity to lower sheet resistance. For a fair comparison, we standardized the treatment duration to 1 minute for all concentrations, aligning with the widely accepted principle that higher acid concentrations typically yield greater effectiveness. Table 3 displays the study's findings. The 1×P-S samples demonstrated that a 100% concentration of HNO_3 produced the lowest sheet resistance, at 130 Ω/sq. The maximum sheet resistance, 1819 Ω/sq, was obtained at the 20% concentration. Interestingly, sheet resistance results for acid concentrations of 40%, 60%, and 80% ranged from 170 to 200 Ω/sq.

We now compare R_{sq} of P-S stacks treated with 60% HNO_3 to those that were not, taking into account the number of layers in Figure 3 and Table 4. HNO_3 treatment drastically reduced sheet resistance by about two orders of magnitude across all P-S pellicle samples. Notably, the best performance, 7.7 Ω/sq, was obtained by treating 9×lamina P-S layers with 60% HNO_3. It should be noted that this work expands on our previous work [2], expanding the analysis to encompass nine P-S layers instead of the previous maximum of six. Sheet resistance is reduced threefold as a result of the addition of these extra three layers. However, only slight improvements were obtained with further increases in the number of pellicles (more than nine pellicles). Reference [8] states that by selectively eliminating PSS domains, treating P-S laminas with HNO_3 greatly increases conductivity and results in a more ordered, crystalline PEDOT structure. By increasing polaron interactions between PEDOT chains, this rearrangement enhances mobility and carrier concentration. Higher HNO_3 concentrations, such as14 M, decreased the PSS content by more than 60%, as demonstrated by XPS and Raman spectroscopy. This resulted in an increase in conductivity from 1810 S/cm (using 3 M HNO_3) to 4100 S/cm [8]. Lower energy barriers for inter-chain hopping and simpler charge transfer are the causes of the improvement.

Table 2. Sheet resistance R_{sq} of a single-layer P-S treated with HNO_3, $H3PO_4$, and $H2SO_4$ acids, each at 100% concentration.

Enhancement Method	R_{sq} [Ω/sq]
HNO_3 for 2s, 100% 1-layer P-S	172
H_3PO_4 for 2s, 100% 1-layer P-S	1.2 k
H_2SO_4 for 2s, 100% 1-layer P-S	220

Table 3. Shows the sheet resistance in relation to the HNO_3 acid concentration applied for 60 s.

Enhancement method	R_{sq} [Ω/sq]
1-layer P-S + HNO_3 100%,60 s	129
1-layer P-S + HNO_3 80%, 60 s	172
1-layer P-S + HNO_3 60%, 60 s	182
1-layer P-S + HNO_3 40%, 60 s	203
1-layer P-S + HNO_3 20%, 60 s	1832

Integrated Nano, 2026, Vol. X, Iss. X, 60-75
DOI: 10.62184/in.jin010420261

Research Article

Table 4. Shows the sheet resistance, R_{sq}, of multilayer stack of P-S laminas with and without HNO_3 acid treatment.

Numbers of P-S Layers	R_{sq} 60% HNO_3 60 s [Ω/sq]	R_{sq} no acid [Ω/sq]
1-layer P-S	182	231k
3-layer P-S	52	19k
6- layer P-S	21	910
9-layer P-S	7.6	38.05
12-layer P-S	2.3	15.07

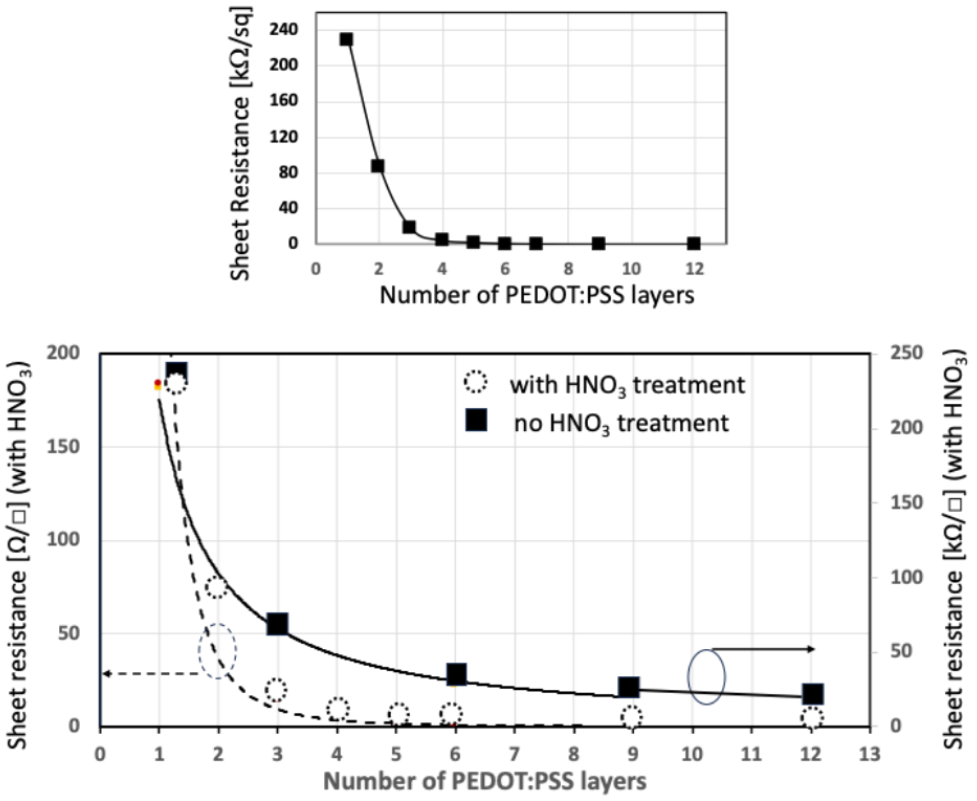

Figure 3. The upper figure depicts the sheet resistance on a linear scale for the multi-layer P-S system untreated by HNO_3 acid. The sheet resistance of the multilayer P-S stack treated with HNO_3, and the untreated stack is contrasted on a logarithmic scale in the lower picture.

Table 5. The sheet resistances (R_{sq}) of 1-layer and 3-layer P-S sheets doped with silver nanoparticles (NP) both topically and in bulk.

Enhancement Technique	R_{sq} [Ω/sq]
1-layer P-S, Ag NP: 0.5 mg/ml in ethanol, topical	464
1-layer P-S, 0.5 mg/ml Ag NP, bulk	628k
3-layer P-S, Ag NP 0.5 mg/ml in ethanol, topical	120
3 × P-S, w/ Ag/NP 0.5 mg/ml, bulk	31k

The increase from six, nine, and twelve layers, particularly when acid treatment is included, implies that the additional three layers are meant to make up for the material loss that occurs during the etching process. A phase separation phenomenon separates the PEDOT and PSS phases in the vertical direction during the spin deposition of P-S, as explained in greater detail elsewhere [2]. The resulting wet lamina collects a PSS-rich solution at the upper segment of the conductive PEDOT chains at the base. As expected, there is a gradual transition between the PEDOT and PSS phases, with the PSS concentration being highest at the top and gradually decreasing towards the bottom. PEDOT exhibits the reverse tendency. With each successive P-S lamina, the PEDOT component of the subsequent lamina penetrates the soluble PSS of the preceding lamina, causing the combined PEDOT phase at the base to thicken and consolidate. The top portion of the layer containing the non-conductive PSS component is eliminated when acid treatment is applied. The conductivity of the etch-reduced P-S lamina should be increased by removing a significant amount of the PSS residues in the PEDOT phase during the acid treatment process.

The study focuses on how Ag NPs might improve P-S's electrical conductivity. Because silver is inert, we applied it in two ways: topical administration following a soft bake of the P-S and bulk doping, in which Ag NPs dispersion is directly combined with P-S solution. Ag NPs in two size ranges 20 to 30 nm and 50 to 60 nm were utilized. The larger nanoparticle sizes consistently produced greater conductivity levels, according to our experiments. Ag NPs topical and bulk uses for 1×lamina and 3×lamina P-S are contrasted in Table 5. Topical application of Ag NPs results in a three orders-of-magnitude increase in sheet resistance compared to the bulk approach. Thus, this approach could prove more advantageous for applications like ReRAM cells, where the inclusion of Cu or Ag is particularly beneficial [1].

The benefit of topical doping is that the metal nanoparticles have a minimal chance of entering the conductive PEDOT phase since they are mostly embedded in the insulating PSS phase at the top of the P-S layer. On the other hand, bulk doping tends to disperse the nanoparticles more evenly across the PEDOT phase and the P-S layer. This uniform distribution, however, can both increase the number of carrier hopping paths and interfere with the alignment and crystallization of the PEDOT chains because the nanoparticle sizes are similar to the thickness of the P-S layer. The conductivity only slightly improves as a result of these conflicting effects.

Topical doping prevents PEDOT chain disruption and significantly increases electrical conductivity in the low-conductivity PSS phase. The finding that the combined effect of topical doping and acid treatment is almost identical to that of either technique alone supports this hypothesis. This implies that the PSS phase, which had been enhanced by metal nanoparticles, is eliminated by the acid treatment, hence nullifying the doping effect.

This implies that bulk doping with nanoparticles is inefficient even when noble metal nanoparticles are included because of various problems like insufficient Ag NPs accommodation within P-S. As far as we know, no studies have been reported to date on the topical application of metal nanoparticles in P-S.

Since bulk doping with silver nanoparticles proved ineffective, we compared the outcomes with topical administration of Cu NPs, a technique we used in our earlier investigation. For three P-S laminas, Cu NPs and Ag NPs yielded comparable sheet resistance values of 173-256 Ω/sq and 121-260 Ω/sq, respectively. Furthermore, for three P-S layers treated with 60% HNO_3 acid, the impacts of both kinds of nanoparticles on sheet resistance were comparable. In light of this, doping with Cu NPs is a more economical choice than doping with Ag NPs. According to existing literature [22, 23], both Ag and Au NPs provide comparable levels of conductivity enhancement in P-S laminas when used in bulk doping. Thus, our previous conclusion about the comparatively low efficacy of bulk doping in comparison to topical doping probably also holds true also for Au NPs. Figure 4 shows the 1-lamina P-S 1500 rpm and 3-lamina P-S doped with Cu NPs using optical microscopy and AFM pictures. The orange shine of the Cu NPs, which range in size from 20 to 30 nm, makes them easily recognized. The rms surface roughness of 1-lamina P-S was 2.01 nm, and for multilamina P-S, the surface roughness rose to 2.42, 2.37, and 2.29 nm for 3-layer P-S, 6-layer P-S, and 9-layer P-S, respectively, based on the AFM measurements.

The distinct surface modifications and interfacial engineering techniques influence the charge transport mechanisms and resulting properties of P-S electrodes through specific and potentially synergistic pathways. The primary mechanism of

acid treatment (e.g. HNO_3) is the reduction of insulating PSS and the structural reorganization of the PEDOT-rich domains. Acid treatment is believed to selectively remove excess PSS and densify the PEDOT phase. This reduces the energy barriers for charge transport by: i) reducing inter-chain and inter-lamellar spacing, facilitating both inter-chain hopping and intra-plane transport. ii) improving the crystallinity and parallel ordering of the PEDOT chains. Since charge transport is fast along the chains but slower between them, this enhanced order significantly improves electron mobility. This effect likely shifts the dominant conduction mechanism toward a more efficient model, such as fluctuation-induced tunneling, by making the conductive pathways more continuous. The incorporation of metallic nanoparticles like Ag NPs primarily enhances conductivity by providing new charge transport pathways: i) they act as additional hopping sites within the polymer matrix, which enhances the rate of charge carrier hopping described by Mott's variable range hopping (VRH) model. ii) they effectively shorten the tunneling distance between conductive PEDOT domains, making tunneling mechanisms (e.g., charging-energy-limited tunneling) more efficient by lowering the potential barrier between sites.

Inserting a graphene layer introduces a highly conductive, two-dimensional platform at the interface with the oxidized wafer. Its primary role is to provide a continuous, high-mobility pathway for in-plane charge collection and transport. It can bridge PEDOT-rich domains, reducing the number of high-resistance junctions and mitigating the slow transport between lamellar planes in the P-S structure.

An excellent in-depth review of the various mechanisms of electronic transport properties in PEDOT-based materials is given in ref.[24]. The true potential of improving electrical conductivity of P-S lies in the combination of these techniques. For instance: i) acid treatment optimizes the morphology of the P-S layer before Ag NPs deposition, creating a more ordered substrate for the nanoparticles to form an effective percolation network. ii) a graphene layer serves as a stable, conductive backbone. A subsequently deposited and acid-treated P-S multilayer could benefit from the graphene's conductivity for in-plane transport, while the acid treatment optimizes vertical transport within the P-S itself. iii) Ag NPs could be used to "wire" together the interfaces between a graphene layer and an acid-treated P-S film, ensuring efficient charge injection across the different material boundaries.

In conclusion, while acid treatment primarily optimizes the intrinsic P-S morphology, Ag NPs provide extrinsic conductive shortcuts, and graphene offers a macroscopic charge transport highway. Their combined use addresses limitations in charge transport across multiple length scales, potentially leading to superior electrical conductivity and operational stability by creating a more robust and interconnected conductive network.

Finally, we address the markedly greater effectiveness of topical doping with metal nanoparticles compared to bulk doping using the same materials. When silver nanoparticles are applied topically, they predominantly localize within the PSS-rich surface layer, where they enhance conductivity through electronic coupling and tunneling. Acting as discrete conductive islands, they form percolation pathways within the otherwise insulating PSS phase, while also serving as charge injection bridges that shorten tunneling distances between isolated PEDOT-rich domains. This localized modification significantly lowers the resistance of the surface region and facilitates more efficient charge collection or injection from the top contact. In contrast, bulk doping—where nanoparticles are dispersed throughout the film during formulation—often disrupts the self-organization and π–π stacking of PEDOT chains, which are critical for intrinsic charge transport. While bulk doping does introduce additional conductive sites, this benefit is frequently counterbalanced or even outweighed by the resulting morphological disorder, leading to only marginal improvements in overall conductivity. Thus, topical doping represents a targeted enhancement of a known resistive region without compromising the conductive bulk, whereas bulk doping tends to be a trade-off between added pathways and structural degradation.

We now explore the specifics of treating with HNO_3. Different treatment durations and concentrations between 0% and 100% were explored. Between one second and one minute, it was discovered that the efficacy of sheet resistance reduction was mostly independent of treatment duration. A 1-minute baseline method was used to guarantee uniform treatment time and reduce potential human error; 30- and 40-second durations showed comparable outcomes.

Integrated Nano, 2026, Vol. X, Iss. X, 60-75
DOI: 10.62184/in.jin010420261

Research Article

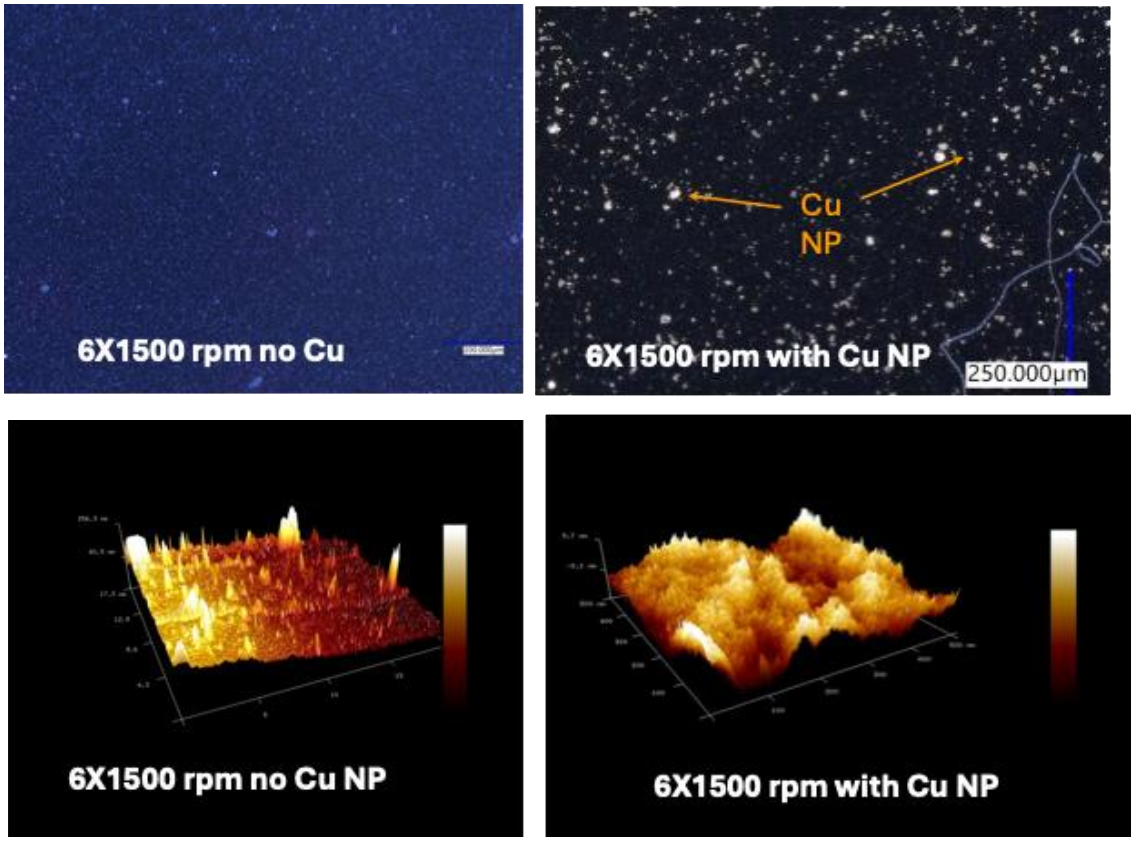

Figure 4. Shows the 6×P-S 1500 rpm without Cu NP and 6× P-S 1500 rpm doped with Cu NPs using optical microscopy and AFM pictures. The whitish shine of the Cu NPs, which range in size from 20 to 30 nm, makes them easily recognized.

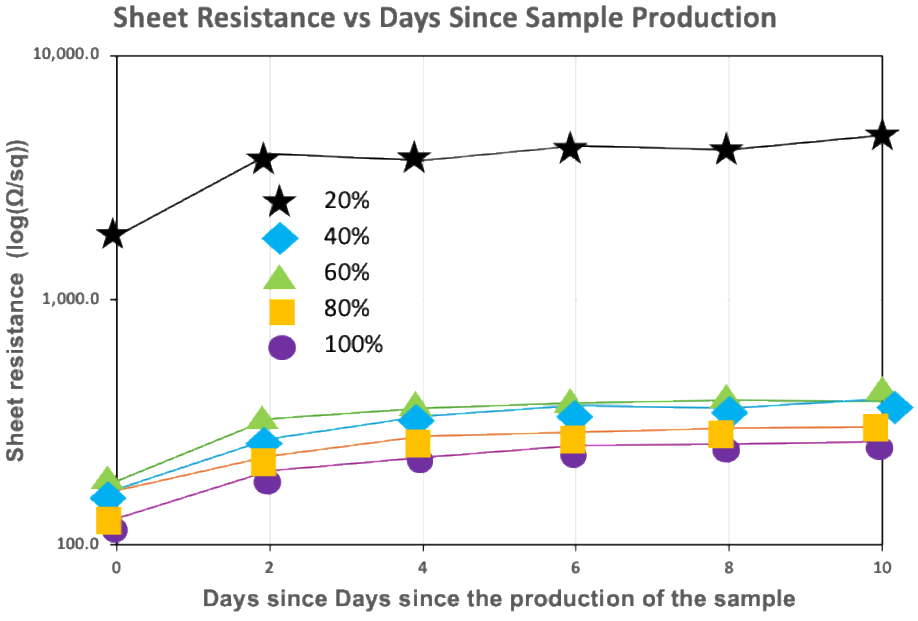

Figure 5. Shows the stability of sheet resistance at 20%, 40%, 60%, and 80% nitric acid concentrations as a function of ambient exposure.

Integrated Nano, 2026, Vol. X, Iss. X, 60-75
DOI: 10.62184/in.jin010420261

Research Article

Furthermore, the long-term stability of nitric acid treatment was evaluated. Sheet resistance was frequently checked while samples were allowed to sit for a few days. Figure 5 provides a graphical representation of the experiment results. As time passes, the degradation of the sheet resistance at all acid concentrations is evident, and after around six days, it reaches saturation and remains constant.

The data are re-graphed in Figure 6, which shows sheet resistance deterioration (D%) as determined by Equation (2):

$$D\% = \frac{Rmeas - Ro}{Ro} \qquad (2)$$

where R_{meas}= the resistance of the sheet on the day of measurement and R_o= the resistance of the sheet immediately following manufacturing.

Figure 6 shows that the sheet resistance performs best steadily at a 60% nitric acid concentration. As a result, for the tests, we employed a baseline technique of 60% nitric acid concentration.

An examination of possible explanations for the unusual phenomenon of sheet resistance degradation after acid treatment was warranted. According to one theory, the degradation could result from an interaction between the acid-treated P-S and the surrounding lab air. In order to verify this hypothesis, we produced identical samples and put some in a small vacuum chamber and others in the typical lab setting. The samples were then taken out of the chamber briefly in order to evaluate the resistance of the sheet.

Figure 7 displays the outcomes for samples stored in the vacuum chamber and in a typical laboratory setting. Remarkably, there was no appreciable difference in sheet resistance between the two values. Consequently, we conclude that rather than a connection between the samples and the ambient air, the degradation is the result of an internal reaction within the P-S material itself. Given the scarcity of nm-thin laminas for this reaction, this observation is accidental. It also explains why, over time, the degradation progressively gets closer to a saturation level.

In the third technique, before applying the P-S layer, graphene was deposited on an oxidized Si wafer to decrease joint P-S/graphene sheet resistance. Triple lamina graphene and a single-large graphene lamina were the two types of graphene that were examined, as indicated in the previous section. At 20 kΩ/sq, the graphene monolayer's sheet resistance was evaluated; at 50 Ω/sq, the trilayer graphene showed noticeably less resistance.

One should keep in mind that using trilayer graphene caused adhesion issues with P-S. We were able to overcome this problem and significantly improve P-S adhesion to the threefold layer graphene by treating it with plasma. However, this increase in adhesion came at a price, since the sheet resistance of the threefold graphene lamina sheet resistance appreciably decreased. Additionally, the graphene trilayer's R_{sq} values for P-S showed a very uneven distribution of sheet resistance, varying across the area of the sample from 14 Ω/sq to 1 kΩ/sq depending on the test site. Notably, plasma treatment of trilayer graphene yielded sheet resistance values as low as 14.3 Ω/sq at the lower end of the range, opening up exciting possibilities for further research.

The lower range of sheet resistance for plasma-treated three-layer graphene is especially remarkable, with values dropping to as low as 14 Ω/sq, presenting exciting opportunities for further research. Since handling three-fold graphene layer is easier than depositing a graphene monolayer onto a substrate, it is still possible to effectively address the non-uniformity issue. It is crucial to understand that three-fold graphene layer necessitates a lamina that is supplied by the supplier on oxidized Si substrates (Graphenea [20]). This places limitations on manufacturing autonomy, especially with regard to commercially available wafer sizes. On the other hand, we fabricated a single 6×P-S sample on a plasma-treated three-layer graphene substrate, achieving a sheet resistance of 1350 Ω/sq. The consistent sheet resistance seen throughout the wafer is a noteworthy benefit of this outcome. Conversely, a single graphene layer covered with nine P-S layers produced a remarkable 36.4 Ω/sq sheet resistance. This value is still surpassed by a 9×P-S sample treated with 60% nitric acid, which achieved a sheet resistance of R_{sq} = 7.68 Ω/sq. However, the best result was obtained with a twelve-layer P-S stack incorporating two HNO_3 etching steps one after the 6th layer and another after the final 12th layer deposition. The resulting sheet resistance was as low as 2.3 Ω/sq, as shown in Table 4.

When graphene is used in a graphene/polymer bilayer, a number of things can boost conductivity overall. There are several benefits to a bilayer made of a polymer and a monolayer of graphene: 1) the high conductivity of graphene

Integrated Nano, 2026, Vol. X, Iss. X, 60-75
DOI: 10.62184/in.jin010420261

Research Article

itself, 2) the complementary layer function of the polymer, 3) enhanced carrier mobility and hopping at the interface, 4) structural synergy, and 5) interface effects. Graphene offers a very effective conductive charge transport channel in a bilayer. By establishing more conductive channels, graphene improves charge transfer in situations when the polymer is conductive, such as P-S. By enhancing mechanical integrity and more evenly spreading the graphene, the polymer can support the graphene even if it has lower conductivity. This helps to maintain a uniform current distribution. Graphene and conductive polymers work together to improve carrier movement inside the polymer matrix. By acting as a bridge, graphene lowers barriers to charge hopping, particularly in polymers with lower intrinsic conductivity by facilitating the free passage of charge carriers like electrons or holes through the bilayer. Polymer is essential for preserving the graphene layer's elasticity and stability, which is especially crucial in flexible electronic applications. Without sacrificing electrical conductivity, the polymer-graphene interaction also enhances the bilayer's mechanical characteristics.

To maximize electrical qualities, the interface between the polymer and graphene is essential. Charge transfer between the two materials is improved and contact resistance is reduced by a properly oriented interface. For instance, different levels of adhesion to the P-S layer in trilayer graphene following plasma treatment may result in uneven sheet resistance. Non-uniform adhesion and interface effects are the cause of this difference, highlighting how crucial it is to have a uniform interface for best results.

While graphene, whether in monolayer or trilayer form, shares some advantages with metal nanoparticles, it does not respond to nitric acid treatment in the same way as Ag NPs do. The nitric acid treatment can be fine-tuned to address both ambient-induced and ambient-independent factors affecting lamina aging and conductivity degradation. A major highlight of this study is the success of a simple method that integrates multiple P-S depositions with a carefully optimized nitric acid treatment, considering both the duration and concentration of the acid exposure. This method provides a simpler and more cost-effective way to enhance P-S conductivity compared to more complex techniques involving metal nanoparticles and graphene layers. The optimized multilayer P-S, treated with the ideal nitric acid concentration, demonstrates a significant reduction in sheet resistance, dropping from 1 MΩ/sq to 2.3 Ω/sq, compared to a single-layer P-S of the same thickness. We previously observed the lowest sheet resistance of 62 Ω/sq using topical dispersion of Cu NPs solution and six P-S layers [6], which is ten times worse than this.

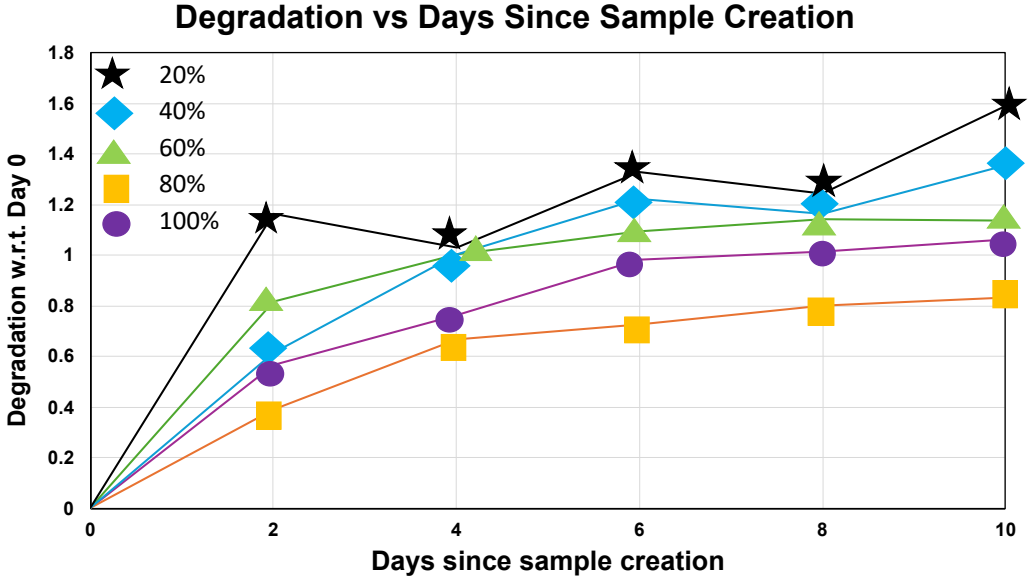

Figure 6. Degradation of sheet resistance at 20%, 40%, 60%, and 80% nitric acid concentrations as a function of ambient exposure.

Integrated Nano, 2026, Vol. X, Iss. X, 60-75
DOI: 10.62184/in.jin010420261

Research Article

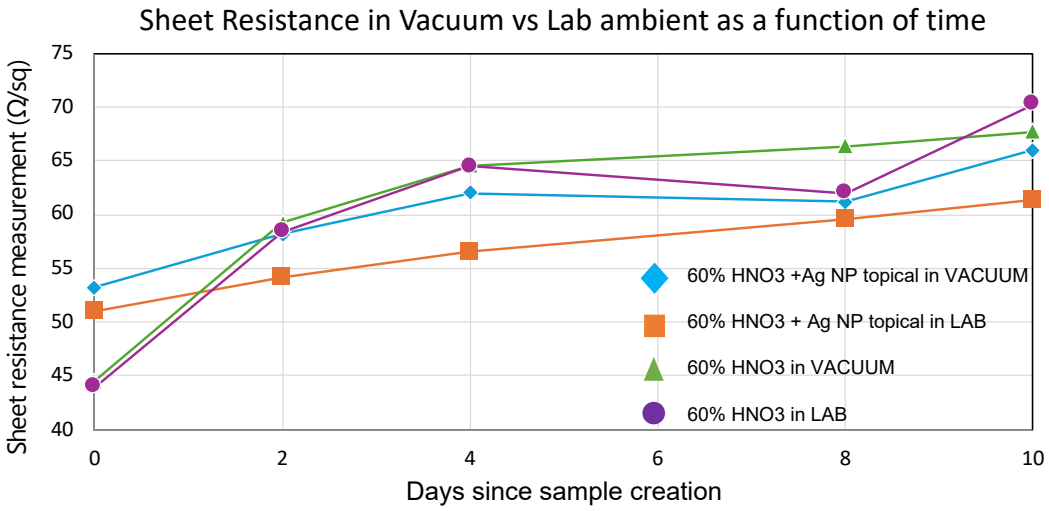

Figure 7. Shows the change in sheet resistance with time (days) for nitric acid treatment at 20%, 40%, 60%, 80%, and 100% HNO_3 concentrations.

Table 6. Comparison of the efficacy of various techniques for enhancing the electrical conductivity of P-S laminas is discussed in this work. (MC-multiple pellicles, AT-acid treatment, NP-doping with nanoparticles, GR-insertion of graphene).

Enhancement Technique	Multiple Pellicles MC	Acid treatment AT	Nanoparticles NP	Graphene GR
Enhancement Efficacy	++++	+++	++	+

Table 7. Synergistic effects of combining various techniques (MC-multiple pellicles, AT-acid treatment, NP-doping with nanoparticles, GR-insertion of graphene).

	MC	AT	NP	GR
MC		+++	++	+
AT	+++		-	+
NP	++	-		+
GR	+	+	+	

Now, let us examine the combined effects of several enhancing strategies. As far as we are aware, there is currently no documentation of the combined effects of using many augmentation techniques. We begin by investigating the relationship between doping with Ag NPs and nitric acid treatment. The results of applying Ag NPs topically are comparable to those of using just HNO_3 treatment, which yields a sheet resistance of 50 Ω/sq for 3×P-S. The use of a recently received P-S has been found to be the cause of an outlier at 25 Ω/sq. Thus, it may be concluded that the effects of nitric acid treatment alone are not appreciably enhanced by the addition of metal nanoparticles.

The concurrent use of graphene insertion and nitric acid treatment is an interesting mix of boosting techniques. Each method significantly reduces sheet resistance when used alone, but their combined benefit seems to be negligible. The inclusion of a graphene monolayer only slightly reduces the R_{sq} to 6.86 Ω/sq. For instance, the sheet resistance of a 12×P-S layer treated with nitric acid is 2.3 Ω/sq. Overall, the best method for increasing P-S conductivity is nitric acid treatment; combinations do not provide any additional advantages.

Moreover, the nitric acid method is both more cost-effective and simpler to implement compared to metal nanoparticle doping and graphene insertion. Table 6 compares the efficacy of various techniques, assessed individually, for enhancing the electrical conductivity of P-S laminas discussed in this work. The results indicate that the most effective methods are multi-pellicle techniques and acid treatment, particularly with HNO_3.

Table 7 presents the potential for synergistic enhancement of electrical conductivity when the enhancement techniques are combined in pairs. The results clearly indicate that the combination of the multipellicle technique with the HNO_3 acid treatment is the most effective and also economically most viable option.

4. Summary and conclusions

We have investigated a number of techniques to improve the electrical conductivity of P-S laminas, such as the insertion of mono - or multi- layer graphene, multiple P-S layer depositions, acid treatments, and metal nanoparticle doping (Cu and Ag). According to our research, while each of these methods considerably improves electrical conductivity when applied separately, no discernible improvements are achieved when combined.

In the realm of Ag NPs and Cu NPs, topical doping has proven to be more successful than bulk doping. Notably, we found that Cu NPs, which are not appropriate for bulk doping, provide a more cost-effective alternative while performing on par with noble metal nanoparticles. Additionally, our optimization efforts led to the development of a nitric acid treatment process that outperforms other methods involving graphene and nanoparticles. Twelve-lamina P-S stacks make up this optimal treatment, which can lower the sheet resistance by more than 10^5 percent, from 1 MΩ/sq to 2.3 Ω/sq. It is important to note, nonetheless, that the electrical conductivity of P-S layers treated with acid deteriorates over time, albeit slowly. This leads to a self-limiting reaction and stabilizes at a constant level after a few days.

Regarding the role of graphene in enhancing conductivity, we discovered that although triple lamina graphene is less expensive than a single graphene layer, it has adhesion problems with the P-S layer. Topical plasma therapy can help with adhesion problems, but it decreases the electrical conductivity gains and affects the homogeneity of sheet resistance. However, awaiting more study and advancement, the triple layer graphene approach offers potential for improving conductivity.

Our investigation into the direct correlation between spin-coating parameters and film properties was performed on silicon wafers to ensure high reproducibility and accurate measurement. The results presented in figures and tables show that these parameters are crucial for determining the thickness and, consequently, the sheet resistance of the multilayer stacks. The feasibility study on Mylar confirms that patterning is possible, but a detailed quantitative analysis on flexible substrates was beyond the scope of this study.

We hope that the insights gained from our investigation into various conductivity-enhancing techniques, as detailed in this publication, will help guide other researchers in selecting the most efficient approaches to enhance electrical conductivity of organic materials for their respective research applications.

Conflict of interest statement

The authors declare that they have no conflict of interest.

Funding statement

The funding grant # 444234 by Semiconductor Research Corporation is acknowledged.

Authors' statement

The authors declare that all the listed authors have made significant contributions to the research and preparation of this manuscript. Specifically, M.O. was responsible for the study design and supervision, A.C. and A.D. conducted the experiments and collected the data, and M.O. performed the data analysis and drafted the manuscript. The remaining authors contributed to some manufacturing in the clean room and electrical characterization of the polymer films. All authors have reviewed and approved the final version of the manuscript. All experiments were conducted in compliance with relevant guidelines and regulations.

We express our gratitude to Prof. Scot Ransbottom and Dr. Don Leber for their invaluable assistance in facilitating this work and providing guidance in navigating clean room issues.

Disclaimer

In this work, no plasma samples from humans have been used.

DOI: 10.62184/in.jin010420261

Research Article

Author information

Corresponding author: Marius Orlowski*

E-mail: m.orlowski@vt.edu

ORCID iD: 0000-0002-1425-4058

Data availability

Data will be available on request.

References

[1] Chakraborty, A., Al-Mamun, M. S., & Orlowski, M. K. (2023). Thermal reliability issues in ReRAM memory arrays. In Memristors - The Fourth Fundamental Circuit Element - Theory, Device, and Applications. Intech Open. https://doi.org/10.5772/intechopen.1001963

[2] Chakraborty, A., Herrera, D., Fallen, P., Hall, D., Bampton, N., Olivero, T., & Orlowski, M. (2023). Conductive organic electrodes for flexible electronic devices. Scientific Reports, 13(1), 4125. https://doi.org/10.1038/s41598-023-30207-9

[3] Groenendaal, L., Jonas, F., Freitag, D., Pielartzik, H., & Reynolds, J. R. (2000). Poly(3,4-ethylenedioxythiophene) and its derivatives: Past, present, and future. Advanced Materials, 12(7), 481-494. https://doi.org/10.1002/(SICI)1521-4095(200004)12:7%3C481::AID-ADMA481%3E3.0.CO;2-C

[4] Kim, Y. H., Sachse, C., Machala, M. L., May, C., Müller-Meskamp, L., & Leo, K. (2011). Highly conductive PEDOT:PSS electrode with optimized solvent and thermal post-treatment for ITO-free organic solar cells. Advanced Functional Materials, 21(6), 1076-1081. https://doi.org/10.1002/adfm.201002290

[5] Xia, Y., & Ouyang, J. (2011). PEDOT:PSS films with significantly enhanced conductivities induced by preferential solvation with cosolvents and their application in polymer photovoltaic cells. Journal of Materials Chemistry, 21(13), 4927–4936. https://doi.org/10.1039/C0JM04177G

[6] Ouyang, J. (2013). Solution-processed PEDOT:PSS films with conductivities as indium tin oxide through a treatment with mild and weak organic acids. ACS Applied Materials & Interfaces, 5(24), 13082-13088. https://doi.org/10.1021/am404113n

[7] Nie, S., Qin, F., Liu, Y., Qiu, C., Jin, Y., Wang, H., ... & Li, Z. (2023). High conductivity, semiconducting, and metallic PEDOT:PSS electrode for all-plastic solar cells. Molecules, 28(6), 2836. https://doi.org/10.3390/molecules28062836

[8] Yeon, C., Yun, S. J., Kim, J., & Lim, J. W. (2015). PEDOT: PSS films with greatly enhanced conductivity via nitric acid treatment at room temperature and their application as Pt/TCO-free counter electrodes in dye-sensitized solar cells. Advanced Electronic Materials, 1(10), 1500121 https://doi.org/10.1002/aelm.201500121

[9] Wang, W., Qin, F., Jiang, X., Zhu, X., Hu, L., Xie, C., ... & Zhou, Y. (2020). Patterning of PEDOT-PSS via nanosecond laser ablation and acid treatment for organic solar cells. Organic Electronics, 87, 105954. https://doi.org/10.1016/j.orgel.2020.105954

[10] Crispin, X., Jakobsson, F. L. E., Crispin, A., Grim, P. C. M., Andersson, P., Volodin, A. V., ... & Berggren, M. (2006). The origin of the high conductivity of poly (3, 4-ethylenedioxythiophene) − poly (styrenesulfonate)(PEDOT− PSS) plastic electrodes. Chemistry of Materials, 18(18), 4354-4360. https://doi.org/10.1021/cm061032+

[11] Kim, D., Shin, K., Kwon, S. G., & Hyeon, T. (2018). Synthesis and biomedical applications of multifunctional nanoparticles. Advanced Materials, 30(49), 1802309. https://doi.org/10.1002/adma.201802309

[12] Okuzaki, H., Takagi, S., Hishiki, F., & Tanigawa, R. (2014). Ionic liquid/polyurethane/PEDOT: PSS composites for electro-active polymer actuators. Sensors and Actuators B: Chemical, 194, 59-63. https://doi.org/10.1016/j.snb.2013.12.059

[13] Zhang, M., Yuan, W., Yao, B., Li, C., & Shi, G. (2014). Solution-processed PEDOT: PSS/graphene composites as the electrocatalyst for oxygen reduction reaction. ACS Applied Materials & Interfaces 6(5), 3587-3593. https://doi.org/10.1021/am405771y

[14] Li, H., Jia, L. P., Ma, R. N., Jia, W. L., & Wang, H. S. (2017). Electrodeposition of PtNPs on the LBL assembled multilayer films of (PDDA-GS/PEDOT: PSS) n and their electrocatalytic activity toward methanol oxidation. RSC Advances, 7(27), 16371-16378. https://doi.org/10.1039/c6ra28784k

[15] Fan, X., Nie, W., Tsai, H., Wang, N., Huang, H., Cheng, Y., ... & Xia, Y. (2019). PEDOT: PSS for flexible and stretchable electronics: Modifications, strategies, and

applications. Advanced Science, 6(19), 1900813. https://doi.org/10.1002/advs.201900813

[16] Chen, H., Xu, H., Luo, M., Wang, W., Qing, X., Lu, Y., ... & Wang, D. (2023). Highly conductive, ultrastrong, and flexible wet-spun PEDOT: PSS/ionic liquid fibers for wearable electronics. ACS Applied Materials & Interfaces, 15(16), 20346-20357. https://doi.org/10.1021/acsami.3c00155

[17] Kim, N., Kee, S., Lee, S. H., Lee, B. H., Kahng, Y. H., Jo, Y. R., ... & Lee, K. (2014). Highly conductive PEDOT: PSS nanofibrils induced by solution-processed crystallization. Advanced Materials, 26(14), 2268-2272. https://doi.org/10.1002/adma.201304611

[18] DiFilippo, A., Chakraborty, A., & Orlowski, M. K. (2024). Towards organic electronics: Enhanced P-S electrode. In Organic Electronics -From Fundamentals to Applications. IntechOpen. https://doi.org/10.5772/intechopen.1007691

[19] Chakraborty, A., DiFilippo, A., Deivasigamani, S., Hong, C., Madwesh, A., & Orlowski, M. (2024). Exploring novel methods: Acid treatment, metal nanoparticle doping, and graphene insertion for enhanced electrical conductivity of nm thin PEDOT: PSS films. Synthetic Metals, 307, 117694. https://doi.org/10.1016/j.synthmet.2024.117694

[20] Graphenea (n.d.). Graphene on your substrate - Processed in ISO 7 cleanroom. https://www.graphenea.com/products/graphene-on-your-substrate

[21] Olivier, J., Servet, B., Vergnolle, M., Mosca, M., & Garry, G. (2001). Stability/instability of conductivity and work function changes of ITO thin films, UV-irradiated in air or vacuum: Measurements by the four-probe method and by Kelvin force microscopy. Synthetic Metals, 122(1), 87-89. https://doi.org/10.1016/S0379-6779(00)01337-0

[22] Patil, D. S., Pawar, S. A., Hwang, J., Kim, J. H., Patil, P. S., & Shin, J. C. (2016). Silver incorporated PEDOT: PSS for enhanced electrochemical performance. Journal of Industrial and Engineering Chemistry, 42, 113-120. https://doi.org/10.1016/j.jiec.2016.07.034

[23] Zhang, R. C., Sun, D., Zhang, R., Lin, W. F., Macias-Montero, M., Patel, J., ... & Maguire, P. (2017). Gold nanoparticle-polymer nanocomposites synthesized by room temperature plasma and their potential for fuel cell electrocatalytic application. Scientific Reports, 7(1), 46682. https://doi.org/10.1038/srep46682

[24] Gueye, M. N., Carella, A., Faure-Vincent, J., Demadrille, R., & Simonato, J. P. (2020). Progress in understanding structure and transport properties of PEDOT-based materials: A critical review. Progress in Materials Science, 108, 100616. https://doi.org/10.1016/j.pmatsci.2019.100616